



The role of bandgap and interface in enhancing photocatalytic H₂ generation activity of 2D-2D black phosphorus/MoS₂ photocatalyst

Yong-Jun Yuan^{a,*}, Pei Wang^a, Zijian Li^a, Yingzhen Wu^a, Wangfeng Bai^a, Yibing Su^b, Jie Guan^{c,*}, Shiting Wu^a, Jiasong Zhong^a, Zhen-Tao Yu^{b,*}, Zhigang Zou^{b,d}

^a College of Materials and Environmental Engineering, Hangzhou Dianzi University, Hangzhou 310018, People's Republic of China

^b National Laboratory of Solid State Microstructures and Collaborative Innovation Center of Advanced Microstructures, Jiangsu Key Laboratory for Nano Technology,

College of Engineering and Applied Science, Nanjing University, Nanjing, 210093, People's Republic of China

^c School of Physics, Southeast University, Nanjing, 211189, People's Republic of China

^d Macau Institute of Systems Engineering, Macau University of Science and Technology, Macau 999078, People's Republic of China



ARTICLE INFO

Keywords:

Black phosphorus
Molybdenum disulfide
2D nanojunctions
Solar hydrogen generation
Broadband light absorption

ABSTRACT

Black phosphorus (BP) has recently emerged as a promising photocatalyst for solar H₂ generation, whereas its bulk crystal with a bandgap of 0.3 eV restricts the driving force for achieving efficient photocatalytic activity. Here, various-sized BP samples were prepared to investigate the role of bandgap in their photocatalytic activities. The results show that the photocatalytic performance of BP samples increases with the decreased layer numbers in the presence of MoS₂ as a cocatalyst, which is related to the more sufficient driving force of fewer-layered BP nanosheets. Furthermore, large and intimate 2D nanojunctions formed in this smart 2D-2D BP/MoS₂ can accelerate the photogenerated charge separation, resulting in the high photocatalytic H₂ production activity. As expected, the 10% BP-10000 nanosheets/MoS₂ photocatalyst exhibits the highest H₂ evolution rate of 1286 $\mu\text{mol}\cdot\text{h}^{-1}\cdot\text{g}^{-1}$ under visible light irradiation ($\lambda > 420$ nm) with an apparent quantum yield of 1.2% at 420 nm, which is much higher than optimized Pt-loaded BP-10000 sample. Moreover, a considerable H₂ generation rate of 341 $\mu\text{mol}\cdot\text{h}^{-1}\cdot\text{g}^{-1}$ is observed under irradiation of the 10% BP-10000 nanosheets/MoS₂ photocatalyst with > 550 nm light. It is further anticipated that this study could provide further insight into the design of efficient BP-based photocatalysts, thus offering extendable availability for the construction of noble-metal-free and visible/near-infrared responsive solar H₂ generation system.

1. Introduction

Solar H₂ generation from water through artificial photosynthesis based on a semiconductor photocatalyst provides an ideal carbon-free hydrogen energy for development of sustainable energy economy [1–3]. A perfect photocatalyst applicable to solar H₂ generation should not only be able to harvest visible light but also low-cost, lowly toxic, and durable in the photocatalytic system. Inspired by the pioneering study of UV-light-responsive TiO₂ electrode for photocatalytic water splitting, [4] numerous narrow-bandgap photocatalysts have been developed, which are primarily metal sulfides [5–7], metal oxides [8–10], and metal (oxy)nitrides [11,12]. Less effort has been devoted to developing metal-free photocatalysts, which are generally more plentiful, cost-efficient and harmfulless as compared to those of metal-based photocatalysts. In 2009, Wang et al., reported the use of graphitic carbon nitride ($\text{g-C}_3\text{N}_4$) as a photocatalyst for H₂ production, which

opens up a new strategy in developing metal-free photocatalysts. [13] During the past 10 years, some other metal-free materials such as red phosphorus, [14] silicon [15], and sulfur have been demonstrated to be active photocatalysts [16], but their photocatalytic performance is still low. Therefore, it is important to further explore metal-free photocatalysts with the aim to improving the apparent quantum yield.

Recently, two-dimensional (2D) black phosphorus (BP) has garnered special attention in materials science field owing to its unique layered structure, high carrier mobility and remarkable in-plane anisotropic electronic properties. [17–21] Significantly, BP exhibits a tunable bandgap which can be tuned from 0.3 eV in the bulk to 2.0 eV in the monolayer by changing the layers. [22] As compared to those commonly-used photocatalysts such as TiO₂, CdS and $\text{g-C}_3\text{N}_4$, the BP nanosheets exhibits a much broader and stronger absorption in the both visible and near-infrared region (NIR), which can harvest much more light to drive photocatalytic H₂ generation reaction. However, there is

* Corresponding authors at: College of Materials and Environmental Engineering, Hangzhou Dianzi University, Hangzhou 310018, People's Republic of China.

E-mail addresses: yjyuan@hdu.edu.cn (Y.-J. Yuan), jieguan@seu.edu.cn (J. Guan), yuzt@nju.edu.cn (Z.-T. Yu).

very little study regarding the use of BP nanosheets as a photocatalyst for photocatalytic water splitting. [23–28] Bulk BP is an ineffective photocatalyst for H₂ production because of the weak driving force for photocatalytic reaction related to the relatively positive conduction band (-0.31 V vs. NHE) and negative valence band (-0.01 V vs. NHE). Expanding the bandgap of BP by decreasing its layers is an effective approach to lower the CB level and raise the VB level, thus the few-layers BP nanosheets with relatively wide bandgap would be promising candidate as a photocatalyst for solar H₂ generation. Therefore, it is of great significance to investigate the effect of bandgap of BP on their photocatalytic performance. In this study, we synthesize various-sized BP samples via a probe sonication assisted liquid exfoliation method, and their photocatalytic activities were investigated in the presence of MoS₂ as a cocatalyst. The MoS₂ was used as a cocatalyst owing to its low-cost and high reactivity for H₂ generation reaction, which has been considered to be the best candidate to replace Pt. [29–38] More importantly, the MoS₂ has a typical 2D structure similar to that of few-layer BP nanosheets, and the combination of MoS₂ and BP nanosheets could form large contact interfaces which provide ample channels for photogenerated charge transfer. The results show that the photocatalytic activity of BP samples increases with the decreasing layer number. Owing to the broad absorption from UV to NIR region of BP and the large interfaces between BP and MoS₂, the optimized BP nanosheets/MoS₂ photocatalyst showed the highest H₂ evolution rate of 1286 μmol h⁻¹ g⁻¹ under visible light irradiation ($\lambda > 420$ nm) with an apparent quantum yield of 1.2% at 420 nm, which is much higher than that of Pt-loaded BP nanosheets photocatalyst. Moreover, a considerable H₂ generation rate of 341 μmol h⁻¹ g⁻¹ was observed under irradiation of the BP nanosheets/MoS₂ with > 550 nm light. This work can open new ways for the design of narrow bandgap and noble-metal-free photocatalysts for solar H₂ generation.

2. Experimental section

2.1. Materials

BP crystal was provided by Nanjing Xianfeng Nanomaterials Technolog Company (Nanjing, China). Ammonium tetrathiomolybdate ((NH₄)₂MoS₄), dimethyl Formamide (DMF), N-methyl-2-pyrrolidone (NMP, 99.5%), absolute ethanol were purchased from Alfa Aesar (Tianjing, China). All the other reagents were chemical reagents and used as received without any further purification.

2.2. Preparation of BP nanosheets

BP nanosheets were prepared by a simple probe sonication assisted liquid exfoliation method. In a typical process, 30 mg bulk crystal powder and 10 mg NaOH were added in 80 ml NMP solution, which was ultrasonicated at temperature below 5 °C for 20 h. Then, the mixed solution was centrifuged at 2500 rpm for 20 min to obtain a BP-25000 sample and a suspension solution of BP nanosheets. The resulted suspension solution was further centrifuged at 10,000 rpm for 20 min to obtain few-layer BP nanosheets as a dark brown solid. The product was washed by deionized water and then freeze-dried.

2.3. Preparation of 2D-2D BP nanosheets/MoS₂ photocatalysts

2D-2D BP nanosheets/MoS₂ photocatalysts were prepared via facile solvothermal method. In a typical process, 30 mg BP sample and 4.87 mg (NH₄)₂MoS₄ were added in 35 ml DMF under stirring. After sonication for 10 min, the mixed solution was transferred into a three-necked round-bottomed flask and then solvothermal treatment at 210 °C for 24 h in the atmosphere of nitrogen. After the autoclave was cooled to room temperature, the resulting black precipitate was collected by centrifugation and then washed with deionized water, and finally freeze-dried to obtain BP/MoS₂ photocatalyst loaded with 10%

MoS₂.

2.4. Characterization

X-ray diffraction patterns were obtained on a Rigaku-miniflex6 X-ray diffractometer with Cu K α radiation ($\lambda = 0.15406$ nm) with an accelerating voltage of 40 kV and a current of 15 mA. Each XRD pattern was scanned through a 2θ range of 10–80° at a step size of 0.2 and a scan rate of 10° min⁻¹. The microstructure of samples was investigated by on a Carl Zeiss Gemini vltra55 field emission scanning electron microscope equipped with an energy dispersive X-rays spectroscopy. The TEM and HRTEM images of samples were performed on a JEOL JEM 2010 transmission electron microscopy using a 200 kV accelerating voltage, and the TEM sample was prepared by drop-casting dispersion onto carbon grid. The thickness of BP nanosheets was obtained on a Multimode 8 (Bruker, USA) atomic force microscopy. The chemical states of samples were studied on a VG ESCALAB MKII X-ray photoelectron spectrometer using a monochromatic Al K α X-ray source, and all the binding energies were calibrated by using the C 1 s peak at 284.8 eV as the reference. The Raman spectrum was recorded on a Horiba LabRam HR Evolution (Japan) microscopic system equipped with a 532 nm laser. UV-vis absorption of solution was performed on an Edinburgh FS5 spectrofluorometer. The UV-vis diffused reflectance spectra were recorded on PerkinElmer LAMBDA 950 UV/Vis spectrophotometer (American). The linear sweep voltammetry curves were performed on a CHI660E electrochemical analyzer (Shanghai ChenhuaLimited, IShanghai) interated with a RRDE-3 A rotating ring disk electrode apparatus in a standard three-electrode cell using a Ag/AgCl (in saturated KCl solution) electrode as the reference electrode, Pt wire as the counter electrode and sample-coated glassy carbon (GC) as the working electrode. The supporting electrolyte was 0.5 M Na₂SO₄ aqueous solution purged with nitrogen.

2.5. Photocatalytic H₂ evolution experiment

Photocatalytic experiments were conducted in a 350 ml Pyrex side-irradiation reaction flash connected to a glass closed circulation system, and the temperature of the reaction solution was below 293 K by a cooling water bath. For each reaction, 10 mg of photocatalyst was well suspended in aqueous solution (250 ml) containing 0.1 M Na₂S and 0.1 M Na₂SO₃ as an electron donor. The reaction solution was evacuated several times to remove the dissolved air completely and then exposed to a 300 W Xenon lamp equipped with a UV cutoff filter ($\lambda > 420$ nm). During reaction process, the evolved H₂ was analyzed in situ by an on-line gas chromatography (CG1690, Jiedao) equipped with a thermal conductivity detector and a column (3 m) of 5 Å molecular sieves, using argon as the carrier gas.

The apparent quantum yield (APY) of photocatalytic H₂ evolution system at 420 nm measured under the same condition except for the wavelength of irradiation light, which was calculated according to the following equations:

$$\eta_{\text{photons}} = \frac{P\lambda}{hc} \times t \quad (1)$$

$$\text{AQY}[\%] = \frac{\text{number of reacted electrons}}{\text{number of incident photons}} \times 100 \\ = \frac{2 \times \text{number of evolved H}_2 \text{ molecules}}{\text{number of incident photons}} \times 100 \quad (2)$$

where P , λ , h , c and t are the incident light power, wavelength of incident light (420 nm), Planck's constant, velocity of light and illumination time, respectively. The power incident light was measured by an optical power meter (Newport 843-R).

3. Results and discussions

The 2D-2D black phosphorus nanosheets/MoS₂ photocatalysts were

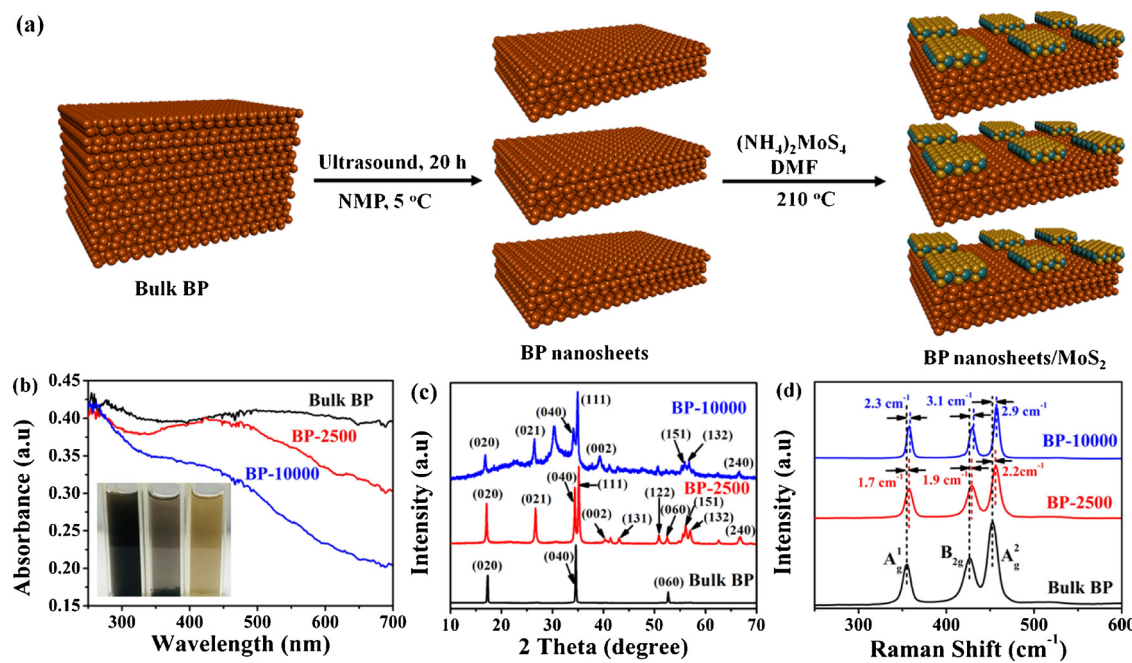


Fig. 1. (a) Schematic diagram of the synthesis of BP/MoS₂ photocatalysts. (b) Absorption spectrum of BP and BP nanosheets suspension (in ethanol solution, 0.1 mg ml⁻¹), the inset is the photograph of bulk BP and BP nanosheets in ethanol solution (0.1 mg ml⁻¹). (c) XRD patterns of bulk BP crystal, BP-2500 and BP-10000 nanosheets. (d) Raman spectrum of bulk BP crystal, BP-2500 and BP-10000 nanosheets.

synthesized by a two-step process as illustrated in Fig. 1a. In the first step, the few-layer BP nanosheets was prepared by liquid exfoliation method containing N-Methyl pyrrolidone (NMP) as a solvent and bulk BP as the raw material at temperature less than 5 °C in an ice bath. The suspension was firstly centrifuged at 2500 rpm to obtain large-sized BP-2500 sample, the resulted solution was further centrifuged at 10,000 rpm to obtain small-sized BP-10000 sample. Then, thermal treatment of $(\text{NH}_4)_2\text{MoS}_4$ and BP nanosheets in anhydrous dimethyl formamide (DMF) led to the form of black phosphorus nanosheets/MoS₂ photocatalysts. UV-vis absorption spectra of various BP samples in ethanol solution are shown Fig. 1b, in which a blue-shift relating to quantum effect occurs when the layer number of BP decreases. That is, a wider bandgap exhibited in the BP nanosheets, which agrees with the color of BP samples change from black to brown (the inset of Fig. 1b) when the layer number of BP decreases. The UV-vis-NIR absorption spectra of solid BP samples were also measured to determine the bandgap of BP samples. As showed in Fig. S1, the bulk BP exhibits a strong light absorption over the whole UV-vis-NIR regions due to its litter bandgap with a value of 0.3 eV. The BP-2500 and BP-10000 samples show relative weaker absorption in the NIR region, and the bandgap of BP-2500 and BP-10000 measured by the curve of $(\alpha h\nu)^2$ versus photon energy was estimated to be approximately 0.77 and 1.32 eV (Fig. S2), respectively. The XRD patterns of original bulk BP in Fig. 1c show three strong diffraction peaks at $2\theta = 17.2^\circ$, 34.5° and 52.8° , which can be indexed to the (020), (040) and (060) planes of BP, respectively. [39] The strongest peak of plane (004) is parallel to the layered structure of BP. After the BP nanoseehts was exfoliated from the bulk crystal, some new diffraction peaks at $2\theta = 26.6^\circ$, 35.2° , 40.3° , 43.3° , 50.9° , 56.3° , 57.1° and 66.7° are observed for BP-2500, which are attributed to the (021), (111), (002), (131), (122), (151), (132) and (240) planes of BP (JCPDS No. 73-1358). [40] As for the BP-10000 nanosheets, the peak intensity ratio of (111) plane to (040) plane increases obviously, suggesting that the dominating (004) plane parallels to the layered structure exhibited in the bulk BP was broken due to the weak Van der Waals forces between the layers. The Raman spectra of different BP samples illustrated in Fig. 1d shows three characteristic Raman peaks of BP, including the out-of-plane vibration mode (A_g^1) and the in-plane vibration modes (B_{2g} and A_g^2) of phosphorus atoms.

[41] It is worth noting that the BP samples show a layer-dependent Raman peaks, that is all Raman peaks shift to the high wave-number with a decreased layers [42].

The morphologies of as-prepared BP nanosheets as well as bulk BP are compared in Fig. 2. As shown in Fig. 2a, the bulk BP with a size large than 20 μm consists of large micrometer-sized scaled sheets that grow together compactly (Fig. S3). After ultrasonic treatment for 24 h, the BP-2500 sample shows two-dimensional features with nonuniform size distribution, some BP sheets have a size of more than 2 μm , and other BP sheets is in the range of 500–2000 nm (Fig. 2b). As for the BP-10000 sample, the SEM image illustrated in Fig. 2c clearly shows its size is less than 500 nm. The TEM analysis further confirm that the BP-2500 is micrometer-scaled (Fig. 2d) while the BP-10000 sample is nanometer-sized (Fig. 2e). The HRTEM image of BP-10000 in Fig. 2f shows the visible lattice fringes with an interplaner distance of 0.26 nm, which can be ascribed to the (040) plane of BP crystal. [43] AFM ananlysis illustrated in Fig. 2(g) and (h) confirms the few-layer BP-10000 nanosheets has a height of 7–8 nm, suggesting the

sole BP nanosheets consists of 14–16 BP layers since one monolayer thickness of 0.53 nm. [44]

In order to explore changes of BP after loading of MoS₂, XRD, Raman, X-ray photoelectron spectroscopy (XPS), SEM and TEM investigations were performed to obtain more insight into the structure, morphologies of as-prepared BP/MoS₂ samples. The XRD patterns of BP/MoS₂ composites illustrated in Fig. 3(a) shows that no peak of MoS₂ can be observed, which is related to its relative weak intensity as well as small amount. Although the presence of MoS₂ in the BP/MoS₂ composites was not be detected by the XRD analysis, but it can be confirmed by the Raman analysis. The Raman spectrum for BP-10000/MoS₂ composite illustrated in Fig. 3(b) shows several characteristic bands at 355, 432 and 468 cm⁻¹, corresponding to the A_g^1 , B_{2g} and A_g^2 modes of BP, respectively. Significantly, the characteristic in-plane E_{2g} and out-of-plane A_{1g} modes of 2H-MoS₂ were observed at 378 and 402 cm⁻¹ were observed, confirming the presence of 2H-MoS₂ in the composite. [45] The chemical states and composition of the BP-10000/MoS₂ composite were characterized by XPS. The wide scan spectrum in Fig. S4 shows the binding energy peaks at 130.2, 170.2, 229.8 and 530.8 eV, which are attributed to P 2p, S 2p, Mo 3d and O 1s,

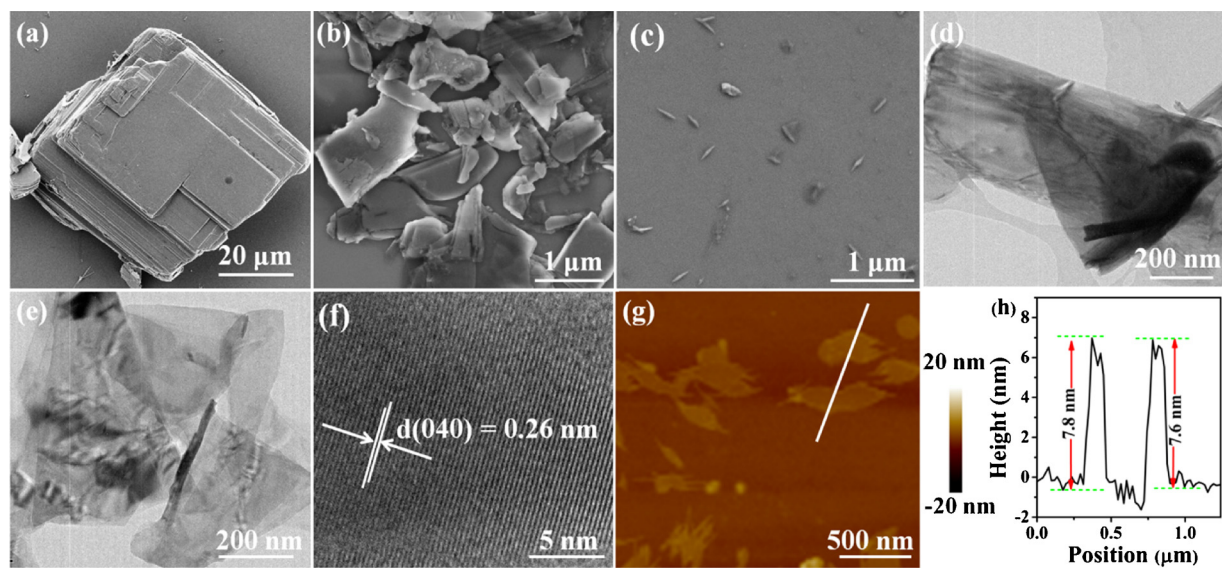


Fig. 2. (a) SEM image of bulk BP. (b) SEM image of BP-2500 nanosheets. (c) SEM image of BP-10000 nanosheets. (d) TEM images of BP-2500 nanosheets. (e) TEM image of BP-10000 nanosheets. (f) HRTEM image of BP-10000 nanosheets. (g) AFM image of 10000 nanosheets. (h) Height profiles along the white line in Fig. 2(g).

respectively. [46,47] The presence of slight O component in the BP-10000/MoS₂ composite could be assigned to the fact that the surface of BP nanosheets can be oxidized during the exfoliation process, which is consistent with previously-reported study. [48] The high-resolution XPS (HR-XPS) spectrum of composite in the P 2p region (Fig. 3c) can be deconvoluted into four peaks located at 130.2 (P 2p_{3/2}), 131.4 (P 2p_{1/2}), 133.2 (P—O—P bonds) and 134.5 eV (O=P=O) [49]. Fig. 3d reproduces the HRXPS of O 1s, which is related to the presence of P=O (530.6 eV), P—O—P (532.1 eV) and P—OH (533.1 eV) bonds. [40] Fig. 3e shows the HR-XPS spectrum of Mo 3d, where two different peaks are corresponding to Mo 3d_{5/2} (228.9 eV) and Mo 3d_{3/2} (231.4 eV), respectively. [50] A relatively weak peak at 225.5 eV was also observed which corresponds to S 2s of MoS₂ [50]. The HR-XPS spectrum of S 2p illustrated in Fig. 3f consists of doublet peaks at 163.6 and 165.5 eV corresponds to S 2p_{3/2} and S 2p_{1/2}, respectively [51].

The morphologies of as-prepared BP/MoS₂ were then analyzed by SEM and TEM. As shown in Fig. 4(a) and S5, there are plentiful MoS₂

nanoflakes that are aggregated together on the surface of bulk BP, and the MoS₂ on BP surface has a similar morphology as that of bare MoS₂ nanosheets (Fig. S6). As for the BP-2500/MoS₂ (Fig. 4b and Fig. S7) and BP-10000/MoS₂ samples (Fig. 4c and Fig. S8), the MoS₂ nanosheets are homogeneously dispersed on the surface of BP without any aggregated MoS₂, which could be assigned to the interaction between the MoS₂ precursors and the oxygen on the exfoliated BP nanosheets. [52] In particular, BP-2500/MoS₂ and BP-10000/MoS₂ samples exhibit intimate and large contact

interfaces as well as abundant exposed edges, which would be key factors in improving their photocatalytic performance for H₂ production. Fig. S9 shows the SEM and corresponding elemental mapping images, which confirmed that Mo, and S elements were distributed on the BP nanosheets surface. The morphologies of as-prepared BP/MoS₂ samples were further characterized by TEM and HRTEM. The TEM images of BP-2500 sample illustrated in Fig. 4(d) and (e) verifies that the layered MoS₂ are grown on the surface of BP nanosheets

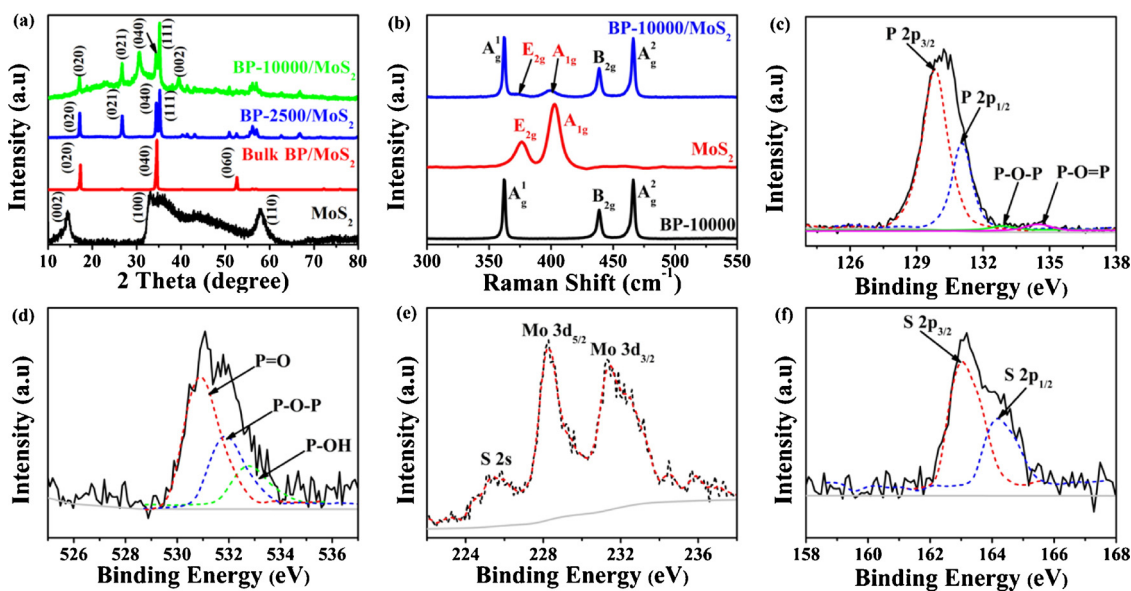


Fig. 3. (a) XRD patterns of MoS₂ and 10% BP/MoS₂ composites; (b) Raman spectrum of 10% BP-10000, MoS₂ and 10% BP-10000/MoS₂. (c–f) High-resolution XPS spectra of P 2p (c), O 1s (d), Mo 3d (e) and S2p (f) BP-10000/MoS₂ (10% MoS₂).

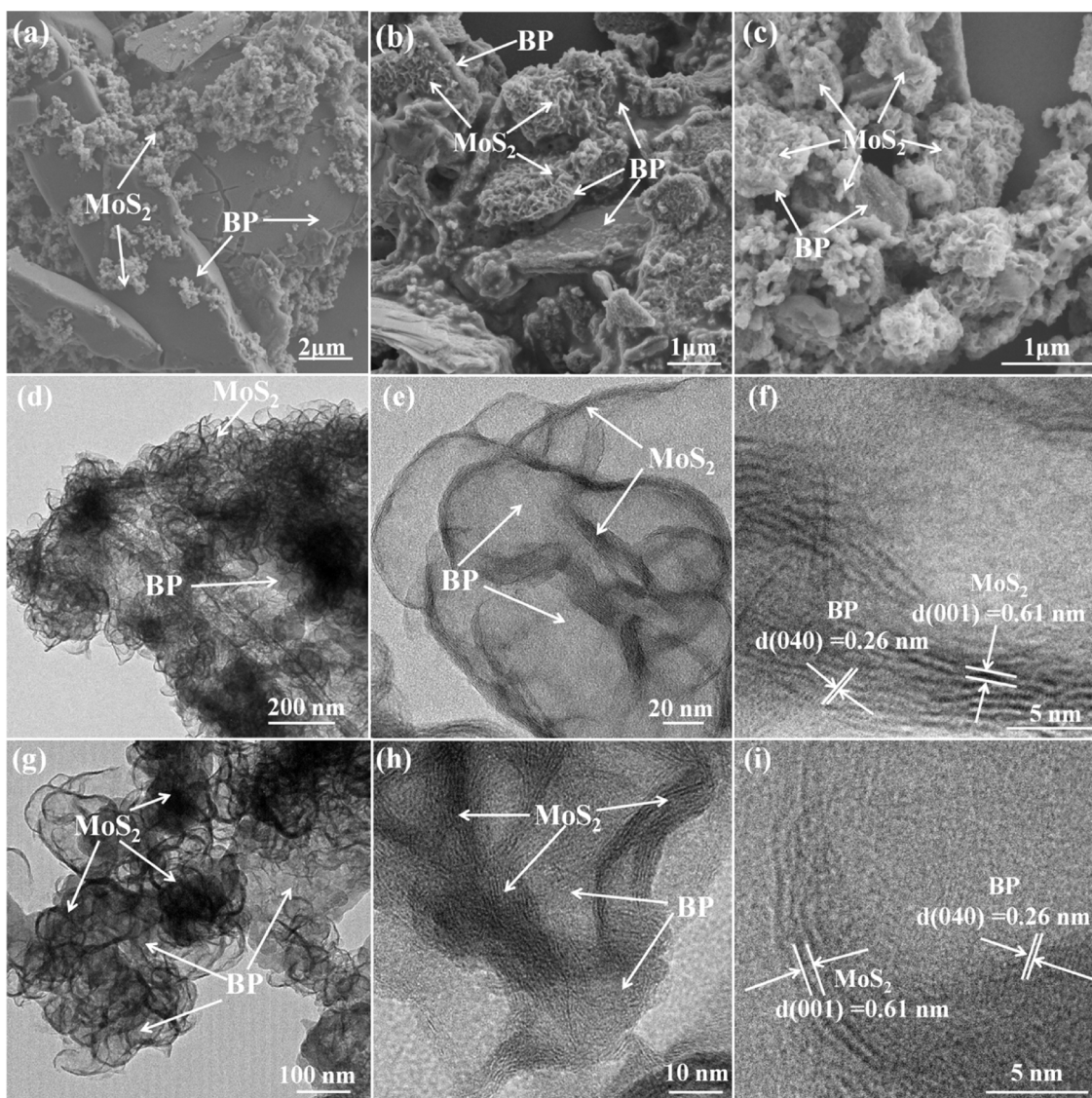


Fig. 4. (a) SEM image of 10% bulk BP/MoS₂ sample. (b) SEM image of 10% BP-2500/MoS₂ sample. (c) SEM image of 10% BP-10000/MoS₂ sample. (d,e) TEM images of 10% BP-2500/MoS₂ sample. (f) HRTEM image of 10% BP-2500/MoS₂ sample. (g,h) TEM images of 10% BP-10000/MoS₂ sample. (i) HRTEM image of 10% BP-10000/MoS₂ sample.

compactly, and the layer numbers of MoS₂ are estimated to be approximately 5–8. From the HRTEM image shown in Fig. 4(f), the lattice fringes of (001) plane with an interplanar distance of 0.61 nm and (040) plane with an interplanar distance of 0.26 nm are assigned to MoS₂ and BP, respectively. [43,53] As for the BP-10000/MoS₂ composite, the TEM images (Fig. 4g, h and i) show that the size of MoS₂ nanosheets are around 5–10 nm connecting to BP surface. The SEM and TEM analysis confirm the successful preparation of 2D-2D BP/MoS₂ photocatalysts.

It is well known that an excellent electrocatalyst is generally potential to be a cocatalyst for photocatalytic H₂ production because the photocatalyst upon irradiation can serve as an electron donor, similar to the applied electric field in electrocatalytic H₂ generation system. Therefore, the electrocatalytic H₂ evolution reaction performance of a catalyst is a criterion to access whether it is competent as a cocatalyst for photocatalytic H₂ production. The catalytic activity of all BP/MoS₂ composites for H₂ generation reaction was evaluated in comparison with MoS₂ nanosheets and bare BP samples. The electrochemical measurements of these catalysts were carried out in 0.5 M sulfuric acid solution using a typical three-electrode system with the loading amount of 0.05 mg·cm⁻² on glassy carbon electrodes. Fig. 5a shows the linear scan voltammetry (LSV) curves of bare BP, MoS₂, BP/MoS₂, BP-2500/

MoS₂ and BP-10000/MoS₂ composites. It is obvious that all BP samples and MoS₂ displayed poor catalytic activity for H₂ generation reaction. After loading the MoS₂ on BP, all BP/MoS₂ samples showed a substantial enhancement in H₂ generation activity. At -0.3 V vs. NHE, the current density of BP/MoS₂ and

BP-2500/MoS₂, was observed to be -1.86 and -3.14 mA, respectively. An expectant current density of 2.88 mA at -0.2 V vs. NHE was observed for BP-10000/MoS₂ sample, which provides important support to explain the high photocatalytic performance of BP-10000/MoS₂ sample, as discussed later. These results demonstrate that the MoS₂ grown on the surface of BP could act as an efficient cocatalyst to enhance the hydrogen evolution activity of BP.

Photocatalytic H₂ production performance of as-prepared MoS₂/BP composites as well as different bare BP samples were evaluated under a 300 W Xe lamp equipped with a UV cutoff filter ($\lambda > 420$ nm) using Na₂S/Na₂SO₃ pair as a sacrificial reagent. Control experiments indicate that no appreciable H₂ was evolved in the absence of either irradiation or photocatalyst, suggesting the H₂ evolution reaction is a light-catalyzed process. Without loading a cocatalyst, all bare BP samples exhibit poor photocatalytic performance for H₂ production (Fig. 5b). The bare bulk BP, BP-2500 and BP-10000 sample exhibits a H₂ evolution rate of

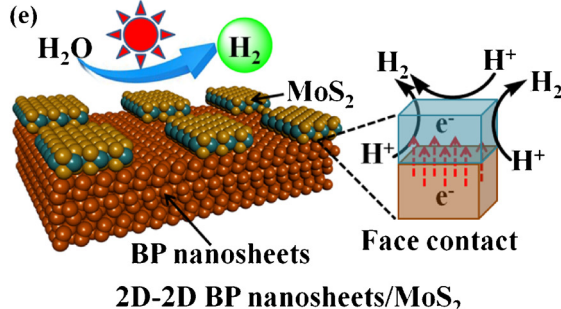
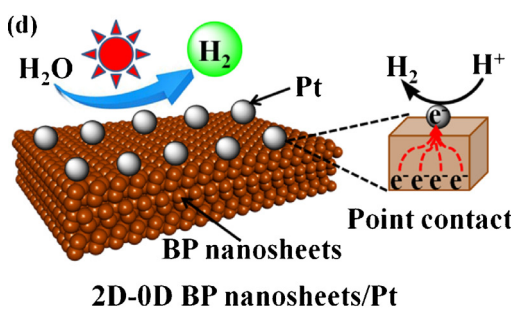
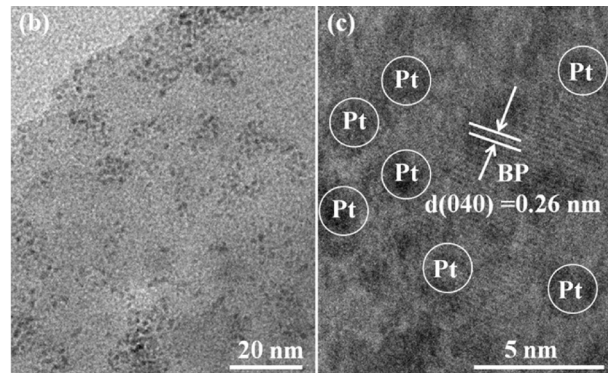
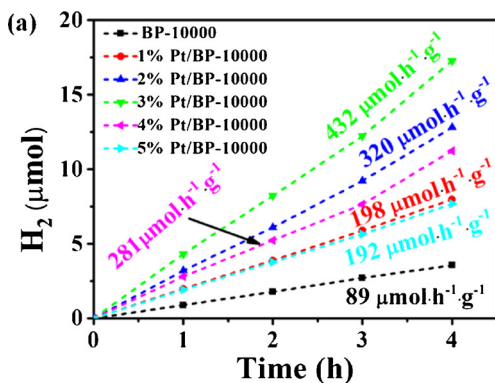
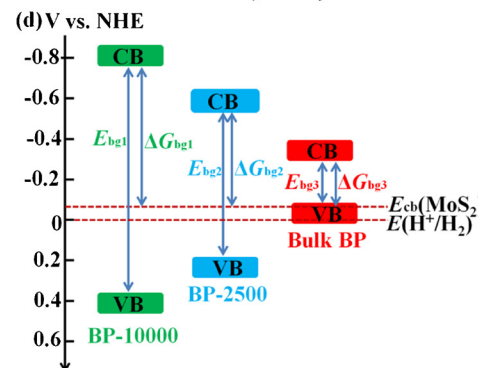
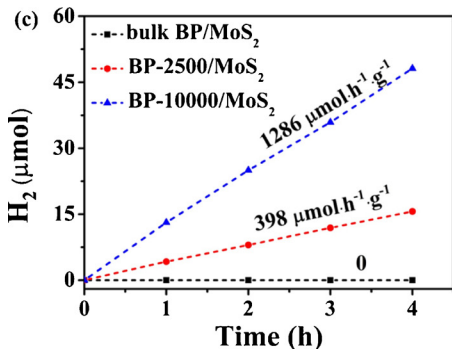
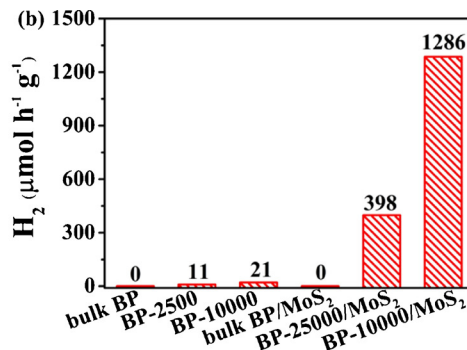
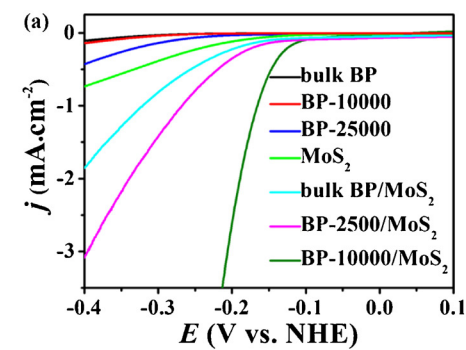


Fig. 6. (a) Photocatalytic H_2 production over different BP-10000/Pt samples under visible light irradiation in neutral aqueous solution in the presence of $0.1\text{ M Na}_2\text{S}$ and $0.1\text{ M Na}_2\text{SO}_3$. (b and c) TEM images of Pt nanoparticles loaded BP-10000 nanosheets. (d and e) Schematic diagrams of 2D-0D BP-10000/Pt and 2D-2D BP-10000/MoS₂ photocatalysts, which clearly shows that the 2D-2D BP-10000/MoS₂ photocatalyst exhibits much larger contact surface interfacial charge transfer in comparison to the 2D-0D BP-10000/Pt photocatalyst.

0, 11 and 21 $\mu\text{mol h}^{-1} \text{g}^{-1}$, respectively. After loading 10% MoS₂, the bulk BP is still an inactive photocatalyst but the H_2 evolution rate of BP-2500 and BP-10000 sample was enhanced to 398 and 1286 $\mu\text{mol h}^{-1} \text{g}^{-1}$ (Fig. 5c), respectively. Both bulk BP alone and bulk BP/MoS₂ showed negligible photocatalytic performance toward H_2 production, which could be attributed to the mismatched band energy. Because of all BP samples exhibit strong and broad light absorption from UV to NIR

region, the change of light-absorption capability was not the crucial factor leading to the enhanced photocatalytic activity, and the band edge position of BP samples is more significant factor influencing the H_2 evolution activity. As shown in Fig. 5d, the bulk BP with a bandgap of 0.3 eV has a conduction and valance band level at -0.31 V and -0.01 V, respectively. [40,54] Although the CB level of bulk BP is suitable for H_2 production, its VB level is close to the redox potential of H^+/H_2 ,

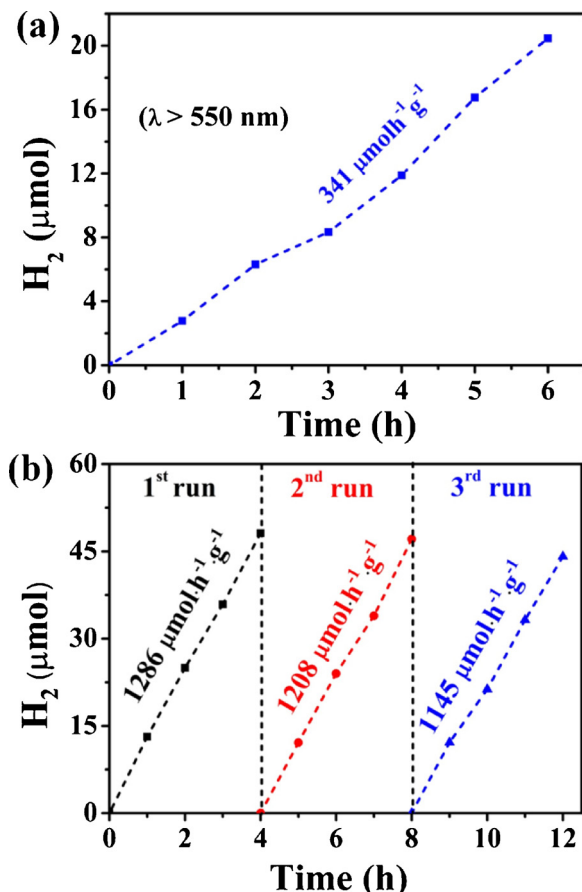


Fig. 7. (a) Photocatalytic H₂ generation curves for 10 mg BP-10000/MoS₂ in 250 ml 0.1 M Na₂S and 0.1 Na₂SO₃ aqueous solution under $\lambda > 550$ nm irradiation. (b) Cyclic H₂ evolution curve for BP-10000/MoS₂ sample in neutral aqueous solution in the presence of 0.1 M Na₂S and 0.1 Na₂SO₃.

resulting in the high recombination efficiency of photogenerated electron-hole pairs and the negligible photocatalytic activity for H₂ generation. Owing to the quantum confinement of the nanosized BP nanosheets, the CB level of BP nanosheets lower to the more negative with the decreased BP layer, providing more sufficient driving force (ΔG) for photocatalytic H₂ production reaction. The driving force plays an important factor in enhancing the photocatalytic performance for H₂ production. Therefore, the BP-10000 and BP-10000/MoS₂ samples exhibit much higher photocatalytic performance than that of BP-2500 and BP-2500/MoS₂, respectively. The maximal H₂ evolution rate up to 1286 μmol h⁻¹ g⁻¹ with an apparent quantum yield of 1.2% at 420 nm was obtained for BP-10000/MoS₂, which is 62 times higher than that of bare BP-10000. Meanwhile, this extremely high H₂ evolution rate is also higher than those previously reported BP/g-C₃N₄ (427 μmol h⁻¹ g⁻¹), [25] Pt/BP (447 μmol h⁻¹ g⁻¹), [28] and Co/BP (694 μmol h⁻¹ g⁻¹) [55] photocatalysts under visible light irradiation ($\lambda > 420$ nm).

For comparison, Pt loaded BP-10000 photocatalysts was prepared by *in situ* photo-deposition method and their photocatalytic H₂ production performance were investigated. [28] As shown in Fig. 6a, the highest H₂ evolution rate of 432 μmol h⁻¹ g⁻¹ was obtained by using the 3% Pt/BP-10000 as the photocatalyst, which is still lower than that of BP-10000/MoS₂ sample loaded with 10% MoS₂. To reveal the potential reasons, the Pt-loaded BP-10000 photocatalyst was collected and then characterized by TEM. As shown in Fig. 6b and c, the TEM image of the Pt-loaded BP-10000 photocatalyst shows that the Pt nanoparticles with an average diameter of ca. 2–3 nm are deposited on the surface of BP-10000 nanosheets. From the TEM images of BP-10000/Pt

(Fig. 6a and b) and BP-10000/MoS₂ (Fig. 4d–i), it can be concluded that the Pt-loaded BP-10000 and BP-10000/MoS₂ photocatalysts exhibit typical 0D-2D and 2D-2D structure, respectively (Fig. 6d and e). In this study, the high photocatalytic activity of BP-10000/MoS₂ photocatalyst could be closely related to the unique 2D-2D structure. In this smart structure, the 2D-2D BP-10000/MoS₂ composite exhibits large 2D nanoInterfaces for photogenerated charge transfer, improving the separation efficiency of electron-hole pairs. Therefore, it is not surprising that the 2D-2D BP-10000/MoS₂ photocatalyst exhibits much higher H₂ evolution performance than those of Pt loaded BP-10000 composites.

The absorption spectrum of B-10000 sample (Fig. S1) shows broad and strong absorption in both visible and near-infrared regions, indicating the possibility of long wavelength light driven photocatalytic H₂ evolution. Fig. 7(a) shows the photocatalytic activity of BP-10000/MoS₂ composite under long wavelength light irradiation ($\lambda > 550$ nm), 20.46 μmol H₂ is produced after 6 h of irradiation, and the H₂ generation rate was estimated to be 341 μmol h⁻¹ g⁻¹.

The result indicates the BP-10000/MoS₂ composite is excellent visible-light-responding photocatalysts for H₂ production. The stability of the BP-10000/MoS₂ photocatalyst was studied by performing recycle experiments under the same reaction conditions. As shown in Fig. 7(b), the H₂ evolution rate of BP-10000/MoS₂ photocatalyst decreased slightly and remained 92% of the initial rate after 3cycles, suggesting the relatively high stability of BP/MoS₂ composite for H₂ production. Previously studies have shown that the BP nanosheets could be oxidized by oxygen dissolved in adsorbed water during the photocatalytic H₂ evolution reactions, resulting in the decreased H₂ evolution rate. [42,54] In this study, the high durability of BP-10000/MoS₂ photocatalyst could be closely related to the close combination between MoS₂ and BP nanosheets. That is, the MoS₂ grown on the surface of BP can act as a contact inhibitor which could hinder the contact between BP and oxygen dissolved in adsorbed water. Base on these above results, a possible reaction mechanism for the enhanced photocatalytic H₂ evolution performance of BP/MoS₂ nanosheets photocatalyst is proposed and the schematic diagram is illustrated in Fig. 6e. Firstly, BP nanosheets can be excited by visible and NIR light to generate photogenerated electrons and holes. Then, the photogenerated electrons can transfer to MoS₂ because the CB position of BP nanosheets is lower than that of MoS₂ nanosheets, [40,56] and then the electrons would react with the adsorbed protons to evolve H₂ at the edge sites of MoS₂ [57]. On the other hand, the sacrificial reagents are oxidized by the photogenerated holes in the VB of BP nanosheets to regenerate the neutral photocatalyst. During these processes, the MoS₂ act as both an electron sink and a cocatalyst which will greatly reduce the recombination of electron-hole pairs and accelerate the H₂ evolution rate, resulting in the excellent photocatalytic activity and high stability of BP/MoS₂ nanosheets photocatalyst.

4. Conclusion

Various-sized BP samples prepared via a probe sonication assisted liquid exfoliation method were used to construct 2D-2D BP nanosheets/MoS₂ photocatalysts for solar H₂ generation. The fewer layered BP nanosheets exhibits much wider bandgap, which provides more sufficient driving force for photocatalytic H₂ production reaction, and thus the photocatalytic performance of BP samples increases with the decreased layer numbers. Owing to the broad absorption from UV to NIR region of BP and the large interfaces between BP and MoS₂, the BP-10000/MoS₂ photocatalyst loaded with 10% MoS₂ showed the highest H₂ evolution rate of 1286 μmol h⁻¹ g⁻¹ under visible light irradiation ($\lambda > 420$ nm) with an apparent quantum yield of 1.2% at 420 nm. Moreover, the 10% BP-10000/MoS₂ sample shows much higher photocatalytic activity than that of optimized Pt loaded BP-10000 photocatalyst. This study can open new ways for the developing narrow bandgap and noble-metal-free photocatalysts with the potential application in the solar H₂ generation.

Conflict of interest

The authors declare no competing financial interest.

Acknowledgements

This research was supported by the National Natural Science Foundation of China under Grant No. 51772071 and 51502068.

Appendix A. Supplementary data

Supplementary material related to this article can be found, in the online version, at doi:<https://doi.org/10.1016/j.apcatb.2018.09.100>.

References

- [1] Y. Wang, H. Suzuki, J. Xie, O. Tomita, D.J. Martin, M. Higashi, D. Kong, R. Abe, J. Tang, *Chem. Rev.* 118 (2018) 5201–5241.
- [2] Y.J. Yuan, Z.T. Yu, D.Q. Chen, Z.G. Zou, *Chem. Soc. Rev.* 46 (2017) 603–631.
- [3] G. Zhou, Y. Shan, Y. Hu, X. Xu, L. Long, J. Zhang, J. Dai, J. Guo, J. Shen, S. Li, L. Liu, X. Wu, *Nat. Commun.* 9 (2018) 3366.
- [4] A. Fujishima, K. Honda, *Nature* 238 (1972) 37–38.
- [5] K. Zhang, J.K. Kim, M. Ma, S.Y. Yim, C.L. Lee, H. Shin, J.H. Park, *Adv. Funct. Mater.* 26 (2016) 4527–4534.
- [6] Z. Jiang, J. Liu, M. Gao, X. Fan, L. Zhang, J. Zhang, *Adv. Mater.* 29 (2017) 1603369.
- [7] Y.J. Yuan, D.Q. Chen, Z.T. Yu, Z.G. Zou, *J. Mater. Chem. A Mater. Energy Sustain.* 6 (2018) 11606–11630.
- [8] X. Wang, Q. Xu, M. Li, S. Shen, X. Wang, Y. Wang, Z. Feng, J. Shi, H. Han, C. Li, *Angew. Chem. Int. Ed.* 51 (2012) 13089–13092.
- [9] Z.Y. Lin, J. Xiao, L.H. Li, P. Liu, C.X. Wang, G.W. Yang, *Adv. Energy Mater.* 6 (2016) 1501865.
- [10] J. Núñez, F. Fresno, A.E. Platero-Prats, P. Jana, J.L.G. Fierro, J.M. Coronado, D.P. Serrano, V.A. de la Peña, O'Shea, *ACS Appl. Mater. Interfaces* 8 (2016) 23729–23738.
- [11] C. Pan, T. Takata, M. Nakabayashi, T. Matsumoto, N. Shibata, Y. Ikuhara, K. Domen, *Angew. Chem. Int. Ed.* 54 (2015) 2955–2959.
- [12] C. Pan, T. Hisatomi, Q. Wang, S. Chen, Ma. Nakabayashi, N. Shibata, C. Pan, T. Takata, M. Katayama, T. Minegishi, A. Kudo, K. Domen, *ACS Catal.* 6 (2016) 7188–7196.
- [13] X. Wang, K. Maeda, A. Thomas, K. Takanabe, G. Xin, J.M. Carlsson, K. Domen, M. Antonietti, *Nat. Mater.* 8 (2009) 76–82.
- [14] F. Wang, W.K.H. Ng, J.C. Yu, H. Zhu, C. Li, L. Zhang, Z. Liu, Q. Li, *Appl. Catal. B: Environ.* 111–112 (2012) 409–414.
- [15] D. Liu, L. Li, Y. Gao, C. Wang, J. Jiang, Y. Xiong, *Angew. Chem. Int. Ed.* 54 (2015) 2980–2985.
- [16] G. Liu, P. Niu, L. Yin, H.M. Cheng, *J. Am. Chem. Soc.* 134 (2012) 9070–9073.
- [17] J. Kim, S.S. Baik, S.H. Ryu, Y. Sohn, S. Park, B.G. Park, J. Denlinger, Y. Yi, H.J. Choi, K.S. Kim, *Science* 349 (2015) 723–726.
- [18] A. Avsar, J.Y. Tan, Kurpas M, M. Gmitra, K. Watanabe, T. Taniguchi, J. Fabian, B. Özilmez, *Nat. Phys.* 13 (2017) 888–893.
- [19] Z. Sofer, D. Sedmidubský, Š. Huber, J. Luxa, D. Bouša, C. Boothroyd, M. Pumera, *Angew. Chem. Int. Ed.* 55 (2016) 3382–3386.
- [20] B.C. Deng, V. Tran, Y.J. Xie, H. Jiang, C. Li, Q. Guo, X.M. Wang, H. Tian, S.J. Koester, H. Wang, J.J. Cha, Q.F. Xia, L. Yang, F.N. Xia, *Nat. Commun.* 8 (2017) 14474.
- [21] R. Gusmão, Z. Sofer, M. Pumera, *Angew. Chem. Int. Ed.* 56 (2017) 8052–8072.
- [22] V. Tran, R. Soklaski, Y. Liang, L. Yang, *Phys. Rev. B* 89 (2014) 235319.
- [23] M. Zhu X.Cai.M. Fujitsuka, J. Zhang, T. Majima, *Angew. Chem. Int. Ed.* 56 (2017) 2064–2068.
- [24] B. Tian, B. Tian, B. Smith, M.C. Scott, R. Hua, Q. Lei, Y. Tian, *Nat. Commun.* 9 (2018) 1397.
- [25] M. Zhu, S. Kim, L. Mao, M. Fujitsuka, J. Zhang, X. Wang, T. Majima, *J. Am. Chem. Soc.* 139 (2017) 13234–13242.
- [26] M. Zhu, Z. Sun, M. Fujitsuka, T. Majima, *Angew. Chem. Int. Ed.* 57 (2018) 2160–2164.
- [27] J. Ran, B. Zhu, S.Z. Qiao, *Angew. Chem. Int. Ed.* 56 (2017) 10373–10377.
- [28] B. Tian, B. Tian, B. Smith, M.C. Scott, Q. Lei, R. Hua, Y. Tian, Y. Liu, *Proc. Natl. Acad. Sci. U. S. A.* 115 (2018) 4345–4350.
- [29] Y.J. Yuan, Z.J. Ye, H.W. Lu, B. Hu, Y.H. Li, D.Q. Chen, J.S. Zhong, Z.T. Yu, Z.G. Zou, *ACS Catal.* 6 (2016) 532–541.
- [30] X. Shi, M. Fujitsuka, S. Kim, T. Majima, *Small* 14 (2018) 1703277.
- [31] Y.J. Yuan, Y. Yang, Z.J. Li, D.Q. Chen, S.T. Wu, G.L. Fang, W.F. Bai, M.Y. Ding, L.X. Yang, D.P. Cao, Z.T. Yu, Z.G. Zou, *ACS Appl. Energy Mater.* 1 (2018) 1400–1407.
- [32] S. Zhang, X. Liu, C. Liu, S. Luo, L. Wang, T. Cai, Y. Zeng, J. Yuan, W. Dong, Y. Pei, Y. Liu, *ACS Nano* 12 (2018) 751–758.
- [33] Y.J. Yuan, D.Q. Chen, Y.W. Huang, Z.T. Yu, J.S. Zhong, T.T. Chen, W.G. Tu, Z.J. Guan, D.P. Cao, *Chem. Eng. J.* 350 (2018) 335–343.
- [34] L.L. Wang, X. Liu, J.M. Luo, X.D. Duan, J. Crittenden, C.B. Liu, S.Q. Zhang, Y. Pei, Y.X. Zeng, X.F. Duan, *Angew. Chemie Int. Ed. English* 56 (2017) 7610–7614.
- [35] C.B. Liu, L.L. Wang, Y.H. Tang, S.L. Luo, Y.T. Liu, S.Q. Zhang, Y.X. Zeng, Y.Z. Xu, *Appl. Catal. B: Environ.* 164 (2015) 1–9.
- [36] L.L. Wang, X.D. Duan, G.M. Wang, C.B. Liu, S.L. Luo, S.Q. Zhang, Y.X. Zeng, Y.Z. Xu, Y.T. Liu, X.F. Duan, *Appl. Catal. B: Environ.* 186 (2016) 88–96.
- [37] Y. Li, K. Yin, L.L. Wang, X.L. Lu, Y.Q. Zhang, Y.T. Liu, D.F. Yan, Y.Z. Song, S.L. Luo, *Appl. Catal. B: Environ.* 239 (2018) 537–544.
- [38] Y.Z. Xu, L.L. Wang, X. Liu, S.Q. Zhang, C.B. Liu, D.F. Yan, Y.X. Zeng, Y. Pei, Y.T. Liu, S.L. Luo, *J. Mater. Chem. A Mater. Energy Sustain.* 4 (2016) 16524–16530.
- [39] L. Chen, G. Zhou, Z. Liu, X. Ma, J. Chen, Z. Zhang, X. Ma, F. Li, H. Cheng, W. Ren, *Adv. Mater.* 28 (2016) 510–517.
- [40] X. Zhu, T. Zhang, Z. Sun, H. Chen, J. Guan, X. Chen, H. Ji, P. Du, S. Yang, *Adv. Mater.* 29 (2017) 1605776.
- [41] Y. Xu, Z. Wang, Z. Guo, H. Huang, Q. Xiao, H. Zhang, X. Fei. Yu, *Adv. Opt. Mater.* 4 (2016) 1223–1229.
- [42] J.Y. Xu, L.F. Gao, C.X. Hu, Z.Y. Zhu, M. Zhao, Q. Wang, H.L. Zhang, *Chem. Commun. (Camb.)* 52 (2016) 8107–8110.
- [43] R. He, J. Hua, A. Zhang, C. Wang, J. Peng, W. Chen, J. Zeng, *Nano Lett.* 17 (2017) 4311–4316.
- [44] S. Lin, S. Liu, Z. Yang, Y. Li, T.W. Ng, Z. Xu, Q. Bao, J. Hao, C.S. Lee, C. Surya, F. Yan, S.P. Lau, *Adv. Funct. Mater.* 26 (2016) 864–871.
- [45] X. Fan, P. Xu, Y. Sun Zhou, Y.C. Li, M.A.T. Nguyen, M. Terrones, T.E. Mallouk, *Nano Lett.* 15 (2015) 5956–5960.
- [46] J. Li, C. Chen, S. Liu, J. Lu, W.P. Goh, H. Fang, Z. Qiu, B. Tian, Z. Chen, C. Yao, W. Liu, H. Yan, Y. Yu, D. Wang, Y. Wang, M. Lin, C. Su, J. Lu, *Chem. Mater.* 30 (2018) 2742–2749.
- [47] S. Zhang, X. Liu, C. Liu, S. Luo, L. Wang, T. Cai, Y. Zeng, J. Yuan, W. Dong, Y. Pei, Liu Y, *ACS Nano* 12 (12) (2018) 751–758.
- [48] T. Zhang, Y. Wan, H. Xie, Y. Mu, P.W. Du, D. Wang, X. Wu, H. Ji, L. Wan, *J. Am. Chem. Soc.* 140 (2018) 7561–7567.
- [49] Y.T. Yew, Z. Sofer, C.C. Mayorga-Martinez, M. Pumera, *Mater. Chem. Front.* 1 (2017) 1130–1136.
- [50] L.L. Wang, Q.F. Zhang, J.Y. Zhu, X.D. Duan, Z. Xu, Y.T. Liu, H.G. Yang, B.G. Lu, *Energy Storage Mater.* 16 (2019) 37–45.
- [51] Y.J. Yuan, D. Chen, J. Zhong, L.X. Yang, J.J. Wang, M. Liu, Z.T. Yu, Tu W, Z.G. Zou, *J. Mater. Chem. A: Mater. Energy Sustain.* 5 (2017) 15771–15779.
- [52] X. Zheng, J. Xu, K. Yan, H. Wang, Z. Wang, S. Yang, *Chem. Mater.* 26 (2014) 2344–2353.
- [53] Y.J. Yuan, D. Chen, J. Zhong, L.X. Yang, J.J. Wang, Z.T. Yu, Z.G. Zou, *J. Phys. Chem. C* 121 (2017) 24452–24462.
- [54] A. Favron, E. Gaufrès, F. Fossard, A.L.P. Heureux, N.Y.W. Tang, P.L. Lévesque, A. Loiseau, R. Leonelli, S. Francoeur, R. Martel, *Nat. Mater.* 14 (2015) 826–832.
- [55] Q. Liang, F. Shi, X. Xiao, X. Wu, K. Huang, S. Feng, *ChemCatChem* 10 (2018) 2179–2183.
- [56] T.F. Jaramillo, K.P. Jørgensen, J. Bonde, J.H. Nielsen, S. Horch, *Science* 317 (2007) 100–102.
- [57] K. Chang, M. Li. T. Wang, S. Ouyang, P. Li, L. Liu, Ye Ji, *Adv. Energy Mater.* 5 (2015) 1402279.